Nuclear Instruments and Methods in Physics Research A 636 (2011) S24–S30

Contents lists available at ScienceDirect

Nuclear Instruments and Methods in Physics Research A

journal homepage: www.elsevier.com/locate/nima

Development of n-on-p silicon sensors for very high radiation environments

Y. Unno [f,*], A.A. Affolder [h], P.P. Allport [h], R. Bates [e], C. Betancourt [m], J. Bohm [l], H. Brown [h], C. Buttar [e], J.R. Carter [b], G. Casse [h], H. Chen [a], A. Chilingarov [g], V. Cindro [i], A. Clark [d], N. Dawson [m], B. DeWilde [o], Z. Dolezal [k], L. Eklund [e], V. Fadeyev [m], D. Ferrere [d], H. Fox [g], R. French [n], C. Garcia [q], M. Gerling [m], S. Gonzalez Sevilla [d], I. Gorelov [j], A. Greenall [h], A.A. Grillo [m], N. Hamasaki [p], K. Hara [p], H. Hatano [p], M. Hoeferkamp [j], L.B.A. Hommels [b], Y. Ikegami [f], K. Jakobs [c], S. Kamada [r], J. Kierstead [a], P. Kodys [k], M. Kohler [c], T. Kohriki [f], G. Kramberger [i], C. Lacasta [q], Z. Li [a], S. Lindgren [m], D. Lynn [a], M. Mikestikova [l], P. Maddock [m], I. Mandic [i], S. Marti i Garcia [q], F. Martinez-McKinney [m], R. Maunu [o], R. McCarthy [o], J. Metcalfe [j], M. Mikuz [i], M. Minano [q], S. Mitsui [p], V. O'Shea [e], S. Paganis [n], U. Parzefall [c], D. Puldon [o], D. Robinson [b], H.F.-W. Sadrozinski [m], S. Sattari [m], D. Schamberger [o], S. Seidel [j], A. Seiden [m], S. Terada [f], K. Toms [j], D. Tsionou [n], J. Von Wilpert [m], M. Wormald [h], J. Wright [m], M. Yamada [p], K. Yamamura [r]

[a] *Physics Department, Brookhaven National Laboratory, Bldg. 510A, Upton, NY 11973, USA*
[b] *Cavendish Laboratory, Cambridge University, J J Thomson Avenue, UK-Cambridge CB3 0HE, United Kingdom*
[c] *Physikalisches Institut, Universitaet Freiburg, Hermann-Herder Str. 3, D-79104 Freiburg i.Br., Germany*
[d] *Section de Physique, Universite de Geneve, 24 rue Ernest Ansermet, CH-1211 Geneve 4, Switzerland*
[e] *Department of Physics and Astronomy, University of Glasgow, UK-Glasgow G12 8QQ, United Kingdom*
[f] *Institute of Particle and Nuclear Study, High Energy Accelerator Research Organization (KEK), 1-1 Oho, Tsukuba-shi, Ibaraki-ken 305-0801, Japan*
[g] *Physics Department, Lancaster University, UK-Lancaster LA1 4YB, United Kingdom*
[h] *Oliver Lodge Laboratory, University of Liverpool, P.O. Box 147, Oxford Street, UK-Liverpool L69 3BX, United Kingdom*
[i] *Experimental Particle Physics Department, Jozef Stefan Institute, Jamova 39, P.O. Box 3000, SI-1001 Ljubljana, Slovenia*
[j] *Department of Physics and Astronomy, University of New Mexico, Albuquerque, NM 87131, USA*
[k] *Institute of Particle and Nuclear Physics, Charles University in Prague, V Holesovickach 2, CZ-18000 Praha 8, Czech Republic*
[l] *Institute of Physics, Academy of Sciences of the Czech Republic, Na Slovance 2, CZ-18221 Praha 8, Czech Republic*
[m] *Santa Cruz Institute for Particle Physics (SCIPP), University of California Santa Cruz, Santa Cruz, CA 95064, USA*
[n] *Department of Physics & Astronomy, University of Sheffield, Hounsfield Road, UK-Sheffield S3 7RH, United Kingdom*
[o] *Department of Physics and Astronomy, Stony Brook University, Nicolls Road, Stony Brook, NY 11794-3800, USA*
[p] *Institute of Pure and Applied Sciences, University of Tsukuba, 1-1-1 Tennoudai, Tsukuba-shi, Ibaraki 305-8571, Japan*
[q] *Instituto de Fisica Corpuscular (IFIC), Centro Mixt Univ. de Valencia-CSIC, Apdo. 22085, ES-46071 Valencia, Spain*
[r] *Solid-State Division, Hamamatsu Photonics K.K., 1126-1 Ichino-cho, Higashi-ku, Hamamatsu-shi, Shizuoka 435-8558, Japan*

ARTICLE INFO

Available online 6 May 2010

Keywords:
Silicon
Sensor
Microstrip
p-type
n-in-p
ATLAS
SLHC
Radiation damage

ABSTRACT

We have developed a novel and highly radiation-tolerant n-in-p silicon microstrip sensor for very high radiation environments such as in the Super Large Hadron Collider. The sensors are designed for a fluence of 1×10^{15} neq/cm^2 and are fabricated from p-type, FZ, 6 in. (150 mm) wafers onto which we lay out a single 9.75 cm × 9.75 cm large-area sensor and several 1 cm × 1 cm miniature sensors with various n-strip isolation structures. By evaluating the sensors both pre- and post-irradiation by protons and neutrons, we find that the full depletion voltage evolves to approximately 800 V and that the n-strip isolation depends on the p$^+$ concentration. In addition, we characterize the interstrip resistance, interstrip capacitance and the punch-through-protection (PTP) voltage. The first fabrication batch allowed us to identify the weak spots in the PTP and the stereo strip layouts. By understanding the source of the weakness, the mask was modified accordingly. After modification, the follow-up fabrication batches and the latest fabrication of about 30 main sensors and associated miniature sensors have shown good performance, with no sign of microdischarge up to 1000 V.

© 2010 Elsevier B.V. All rights reserved.

1. Introduction

The most eminent example of a very high radiation environment is the large hadron collider (LHC) and the future super LHC

* Corresponding author. Tel.: +81 29 864 5791; fax: +81 29 864 2580.
E-mail address: yoshinobu.unno@kek.jp (Y. Unno).

0168-9002/$ - see front matter © 2010 Elsevier B.V. All rights reserved.
doi:10.1016/j.nima.2010.04.080

(SLHC). The LHC collects collision data of about 700 fb^{-1} with a nominal luminosity of $10^{34}\,cm^{-2}\,s^{-1}$. The silicon microstrip tracker (SCT) in the inner detector (ID) of the ATLAS detector was built to tolerate an integrated particle fluence of 2×10^{14} (1-MeV neutron-equivalent (neq))/cm^2 at a radius $R\sim30$ cm from the collision point. To maximize its research capabilities, the LHC is to be upgraded to the SLHC, with the goal being to achieve over an order of magnitude higher luminosity ($>10^{35}\,cm^{-2}\,s^{-1}$) and over 4 times more integrated luminosity (3000 fb^{-1}). Fig. 1 shows an expected particle fluence of $\sim10^{15}$ neq/cm^2 at $R\sim30$ cm with $Z\sim150$ cm (along the beamline), with a safety factor of 2 in the luminosity . The ratio of neutrons to charged particles is greater than unity for $R>30$ cm. The neutron fluence is $\sim5\times10^{14}$ neq/cm^2 at $R\sim30$ cm and decreases slightly to $\sim3\times10^{14}$ at $R\sim90$ cm. A large number of pile-up events per beam crossing is foreseen (300–400 compared with 20 at the LHC), so the particle density in the ID will be 15–20 times larger than that at the LHC.

Radiation damage by hadronic particles (pions, protons, neutrons, etc.) creates acceptor-like energy levels in the silicon bulk, causing n-type silicon to mutate into p-type, and increasing the full depletion voltage (FDV) as fluence is accumulated. As a silicon sensor using an n-implant readout in a p-type wafer, the n-in-p sensor offers the following advantages: (1) n-in-p sensors can be fabricated using a single-side lithography process, making them more cost-effective than n-in-n sensors, which require a double-side process. (2) They may be operated in the partially depleted state because the p–n junction is always on the signal-collecting side, making the sensor highly radiation-tolerant. (3) By collecting electrons, a faster signal is obtained and less charge trapping is achieved than by collecting holes.

The surface of the silicon wafer is protected with a silicon oxide layer. At the silicon–silicon oxide interface, the built-in defects and accumulated surface damage due to the ionizing dose will create an excess positive charge leading to an inversion layer of electrons at the surface of the silicon, which shortens the n-implant electrodes. Thus, the silicon surface requires a p^+ layer to prevent the formation of the inversion layer so that the n-strip implants remain isolated. The p^+ layer can be implemented by implanting p-type ions in restricted areas, which is called the p-stop method, or by covering the entire wafer surface with a p^+ layer, which is called the p-spray method. The high-bias voltage required to operate the radiation-tolerant sensor generates a high electric field at the surface structures that will cause the onset of microdischarge, which is a sudden increase in leakage current when the electric field strength exceeds the avalanche breakdown voltage for silicon ($\sim$30 V/μm).

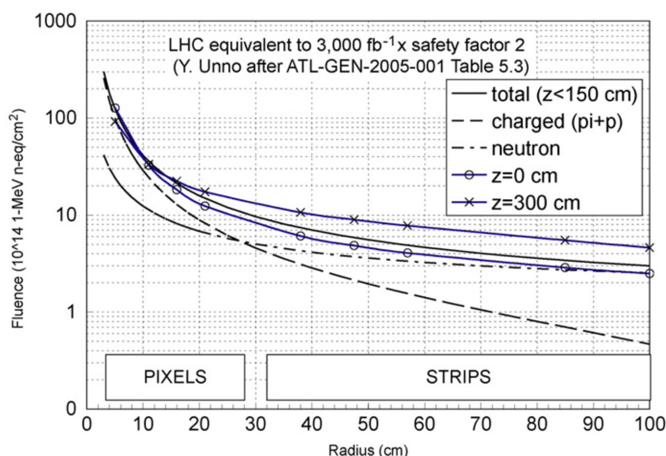

Fig.1. Expected fluences of particles in the inner tracker of the ATLAS detector at SLHC. Values are taken from Ref. [1].

There are several issues involved in developing a highly radiation-tolerant silicon microstrip sensor. A silicon material is needed that has the smallest possible FDV and, especially, an FDV that increases least as a function of fluence. The operational bias voltage must be found that results in the required signal strength. The surface structures must be optimized so that the electric field is minimized, and the necessary concentration of p-type ions in the surface must be determined so that the onset voltage for microdischarge exceeds the operation bias voltage, and yet the n-implant strips remain isolated.

An n-in-p sensor was prototyped for the LHC [2], and significant research has been devoted to the SLHC [3]. For our development [4,5], we have evaluated 4 and 6 in. (100 and 150 mm) silicon wafers, silicon materials incorporating float-zone (FZ) and magnetic Czochralski (MCZ) materials and the wafer orientations of $\langle 1\,0\,0\rangle$ and $\langle 1\,1\,1\rangle$. Most recently, we have fabricated about 50 large-area sensors in a sequence of batches using 6 in. (150 mm) FZ wafers with an orientation of $\langle 1\,0\,0\rangle$.

2. n-in-p R&D sensors

2.1. Large-area main sensor

The mask layout for the 6 in. wafer is shown in Fig. 2. The layout contains a large-area main sensor of dimensions 9.75 cm × 9.75 cm, which is the maximum size square possible in the usable area defined by the vendor [6]. In addition, miniature 1 cm × 1 cm sensors with various strip and isolation structures are included in the layout, as well as 4 mm × 4 mm miniature diodes, which are fit into the space remaining on the wafer. The main sensor is an R&D sensor designed for a high track density environment that has four segments of short strips (2.39 cm each). The top two segments are made with "axial" strips where the strips are parallel to the sensor edge. The bottom two segments are made with "stereo" (i.e., inclined) strips where the strips are rotated by 40 mrad with respect to the sensor edge. The stereo strips are intended for development and verification of the sensor design for a full-area stereo-strip sensor. The strip isolation structure of the main sensor is the one equivalent to the Zone3 of the miniature sensors.

2.2. Miniature sensors

Each miniature sensor (1 cm × 1 cm) has one out of six different surface structures for strip isolation. The cross-sections of the surface structures, Zone 1–Zone 6 (Z1–Z6), are shown in Fig. 3. Z1 has no p-stop structure, Z2 has individual p-stops independently encircling each n-strip and Z3–Z6 have one continuous, common p-stop in between n-strips that are 6 μm wide. The Z1 miniatures become "p-spray-only" if p-spray is applied. The sensors are made with an integrated AC-coupling structure consisting of a sandwich of an insulating layer with aluminium-metal and implant strips. For all the zones except Z5, the metal is wider than the n-strip implant, so that the wider metal functions as a field plate to reduce the electric field strength at the n-strip implant edge when the potential of the metal and the n-strip implant is the same. For comparison, the metal width for Z5 is narrower than the implant. The major features of the R&D sensors are summarized in Table 1.

The fabrication of the sensors was split into a sequence of batches. The first three batches X1–X3 were small in quantity, and the fourth, S1, was the first large-quantity batch. For each batch, we tried the p-stop (P), p-spray (R), or combined isolation methods with p^+ surface-density concentrations ranging from

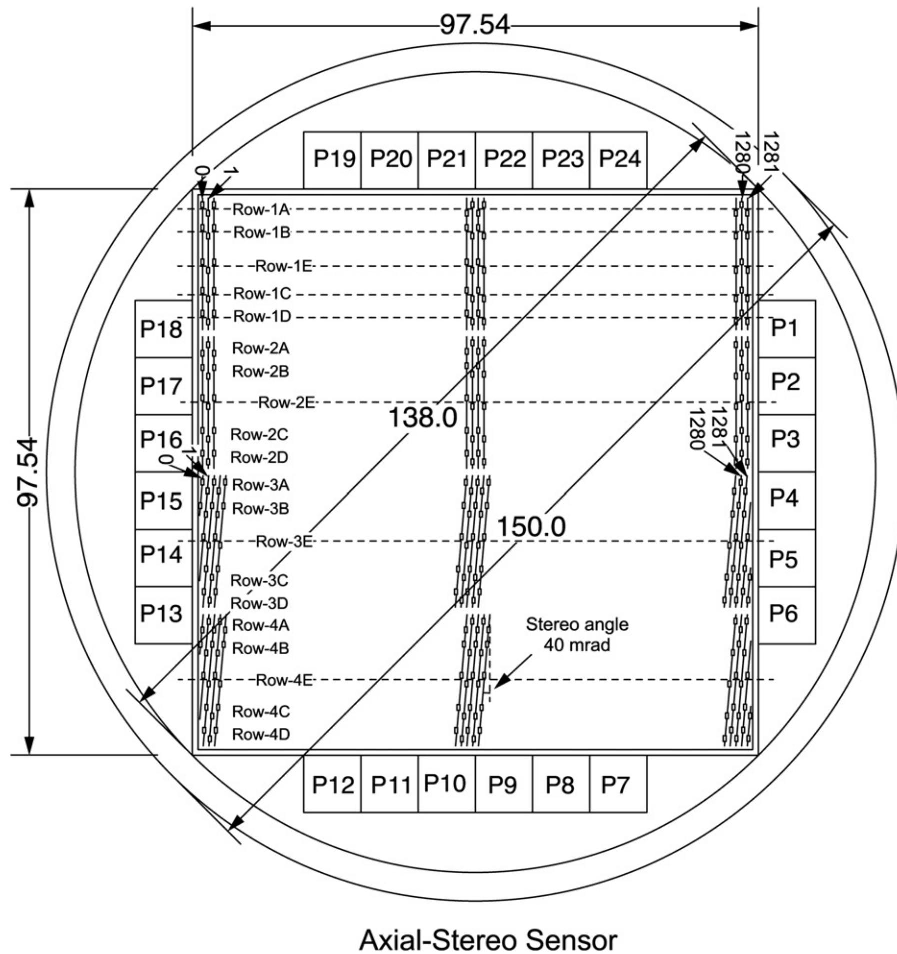

Fig. 2. The layout of the mask for the latest sensors (ATLAS07) for a 150 mm wafer. The central piece is the 9.75 cm × 9.75 cm main sensor and P1–P24 are the miniature sensors of 1 cm × 1 cm.

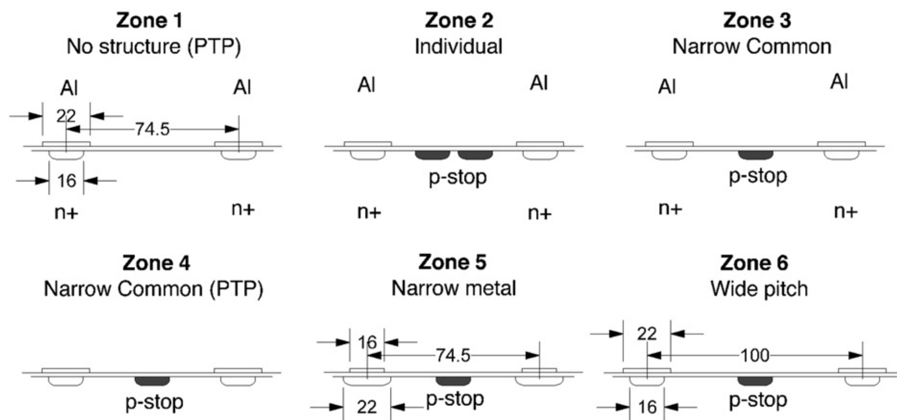

Fig. 3. Cross-sections of the strip (n^+) and the isolation structures (e.g., p-stop) in the surface of the miniature sensors. Six structures, named Zone 1–Zone 6, are implemented—one structure per miniature sensor. The dimensions are in μm.

10^{11} to 10^{13} ions/cm^2. We are foreseeing a batch of p-spray in future. The p-stop and p-spray densities, and the number of wafers delivered for testing are summarized in Table 2. Each batch is named after the sequence and the isolation, e.g., X1R2P8 denotes the first batch with a p-spray density of 2×10^{12} and a p-stop density of 8×10^{12} ions/cm^2, combined. The batches with only p-spray (R) were fabricated by skipping the p-stop process, i.e., there are no p-stop structures in either the main sensor or in any of the miniature sensors in the wafers of the batch.

2.3. Punch-through protection structure

In the Zone 4 (Z4) miniature sensor, we developed a structure for the AC coupling insulator to protect against accidents such as a beam splash into the sensors. When a large amount of charge is deposited in the sensor by a beam splash, a large current flows through the bias resistor and drops the potential of the n-strip implants toward the backplane bias voltage, thus generating a voltage spike across the AC coupling insulator [8]. When the

Table 1
Features of the R&D sensors.

Silicon wafer diameter	6 in. (150 mm)
Type	p-type FZ (high grade)
Orientation	⟨1 0 0⟩
Resistivity (kΩcm)	~6.7
Thickness (μm)	320
Sensor dimension (dicing center–center)	9.75 cm × 9.75 cm
Number of strip segments	4
Number of strips per segment	1282
Strip pitch (μm) (θ: stereo angle)	$74.5 \times \cos(\theta)$
Strip length (cm) (θ: stereo angle)	$2.39/\cos(\theta)$
Stereo angle, θ of "axial"/"stereo" segments (mrad)	0/40
Strip width, implant/metal (μm)	16/22
Distance between bias rail and n-strips implants (μm)	70
Sensor dimension (dicing center–center)	1 cm × 1 cm
Number of strips, Z1–Z5 (Z6)	104 (77)
Strip pitch, Z1–Z5 (Z6) (μm)	74.5 (100)
Strip length (cm)	0.80
Strip width, implant/metal (Z1–Z6), (Z5)	16/22, 22/16
Distance between bias rail and n-strips implants	
(Z1)/(Z2–Z6)/(Z4) (μm)	12/70/20
Sensor position	Z1:(P7,19) Z2:(P2,5,8,14,17,20), Z3:(P1,3,6,9,13,15,18,21) Z4:(A-P4,B-P10,C-P16,D-P22), Z5: (P11,23), Z6:(P12,14)
Interstrip capacitance (one-neighbour-both) (pF/cm)	~0.80 [7]
Body capacitance per strip (pF/cm)	~0.27 [7]
Bias resistance (Polysilicon) (MΩ)	~1.5
Signal readout	AC coupling
AC coupling breakdown voltage (V)	> 100

Table 2
Summary of delivered sensors for testing.

Batch name	P-spray (R) (ions/cm^2)	P-stop (P) (ions/cm^2)	No. of wafers		
			Main	Miniature[a]	Wafer range
X1R2P8	2×10^{12}	8×10^{12}	9	14	1–22
X1P10	–	1×10^{13}	–	9	23–36
X2R2P8	2×10^{12}	2×10^{12}	–	1	1
X2P2	–	2×10^{12}	–	1	25
X2P4	–	4×10^{12}	–	1	31
X2R2	2×10^{12}	–	–	1	35
X3R2P2	2×10^{12}	2×10^{12}	–	3	1–11
X3R2P8	2×10^{12}	8×10^{12}	1	2	46–47
X3P1	–	1×10^{12}	1	1	12–13
X3P2	–	2×10^{12}	6	4	14–31
X3P4	–	4×10^{12}	2	2	32–39
X3R1	1×10^{12}	–	2	1	40–41
X3R2	2×10^{12}	–	1	1	42–43
X3R4	4×10^{12}	–	1	2	44–45
S1P4	–	4×10^{12}	28	15	1–41
S1P10	–	1×10^{13}	1	2	42–45
S1P20	–	2×10^{13}	1	2	46–49

[a] Only those tested by testing sites.

distance between the bias rail and the n-strip implants is appropriate, this voltage between the bias rail and the n-strip implants can be limited by inducing a surface current like the source-drain current of a MOSFET. The protection structure is called the punch-through protection structure (PTP). In the p-stop method, we have investigated a few variations in PTP structures, as shown in Fig. 4. The structure X1Z4 is the first PTP structure implemented in X1, and Z4A–Z4D are the improved designs in batches X2 and later. The reason for the improvement is discussed in Section. 4.

3. Evaluation

3.1. Proton and neutron irradiations

We characterize the R&D sensors both pre- and post-irradiation. Irradiations were made with 70 MeV protons at the Cyclotron and Radioisotope Center (CYRIC) of Tohoku University, Japan [9], and with neutrons with energies below approximately 3 MeV at the TRIGA reactor, at the Jozef Stefan Institute, Slovenia [10]. Typical fluences are 10^{12}, 10^{13}, 5×10^{14} and 10^{15} neq/cm^2. The low fluences are to evaluate the effect of surface damage, e.g., charge-up in the silicon–silicon oxide interface before bulk damage becomes imminent. The high fluence is to evaluate the bulk and surface damage at the ultimate SLHC fluence. Unless otherwise mentioned, the irradiated samples were annealed for 80 min at 60 °C.

3.2. Bulk damage

A study of the bulk damage is presented in Ref. [11]. Evolution of the FDV as a function of fluence is evaluated for the FDVs that are derived from the measurement of the body capacitance C as a function of bias voltage V (C–V) and the measurement of the charge collection as a function of bias voltage using beta rays from ^{90}Sr (CC-V beta). In an ideal semiconductor, $1/C^2$ increases linearly with V. In irradiated sensors, $1/C^2$ exhibits a nonlinearity (i.e., a kink). The FDV estimated from the low bias voltage range is consistent with the FDV estimated from the CC-V(beta) method. The FDVs of proton and neutron irradiations are ~700 V at 10^{15} neq/cm^2 and ~800 V at 5×10^{14} neq/cm^2, respectively.

3.3. Surface damage

Surface damage is presented in Ref. [12]. Strip isolation is evaluated in the miniature sensors of the batch X3 with p-stop only, p-spray only and p-spray and p-stop combined. The pre-irradiation samples all show good isolation resistance of > 10 GΩ. The post-irradiation samples show degraded isolation resistance. The isolation resistance of samples irradiated by protons to 1.14×10^{13} neq/cm^2 is characterized by the total p$^+$ concentration. It is in the 1 MΩ range for 10^{12} ions/cm^2 and in the 10 MΩ range for 2×10^{12} ions/cm^2 and it grows to the 100 MΩ range for 4×10^{12} ions/cm^2 and is greater than 10 GΩ for 1×10^{13} ions/cm^2. The interstrip capacitance changes little after irradiation and is very similar among the various structures and isolation methods. The exception to this finding is the Z5 structure that exhibits an increase in capacitance after irradiation. The punch-through voltage (PTV), defined as the voltage where the PT resistance R_{PT} is equal to the bias resistance R_{bias}, depends on the total p$^+$ concentration and the fabrication method. For the same distance, higher PTV is observed for p-spray than for p-stop. The PTV of non-irradiated samples is in the range of 10–30 V, but it decreases by 5–10 V for low fluences of 10^{12}–10^{13} neq/cm^2 before increasing again for high fluence (10^{15} neq/cm^2) to the same level as for the non-irradiated samples.

4. Mask design improvement

4.1. Onset of microdischarge

With the mask designed for the first batch, X1, we observed the onset of microdischarge in the non-irradiated X1R2P8 samples at bias voltages of 200–400 V. We identified three prominent hot spots using a hot-electron microscope [13]. One

Fig. 4. Punch-through protection structures. Z4A–Z4D are in the improved mask, and X1Z4 is in the original mask.

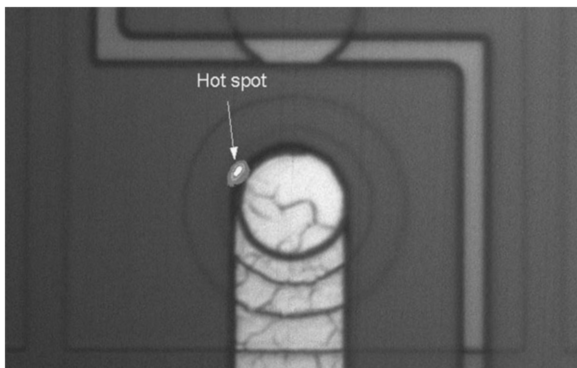

Fig. 5. Hot spot in the X1R2P8 Z4 miniature sensor observed using the hot-electron equipment.

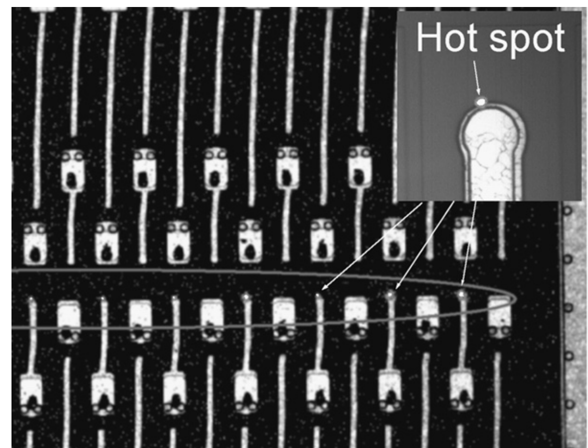

Fig. 6. Hot spots at the corner of the bonding pads of the stereo strips in the X1R2P8 main sensor observed using the hot-electron equipment.

hot spot was in the miniature sensors of X1Z4 at the PTP structure, as shown by spot (1) in Fig. 5. The other two hot spots were in the main sensor in the structure of the "stereo" strip segments. Specifically, hot spot (2) shown in Fig. 6 was at the corner of the bonding pads facing the bias rail, and hot spot (3) was at the end of alternating strips, as shown in Fig. 7. For clarification, graphical drawings of the layout corresponding to the regions of hot spots (2) and (3) are shown in Fig. 8 (a) and (b), respectively. We used a TCAD simulation program [14] to determine the large electric field needed to induce such a microdischarge. A brief conclusion of the study is that multiple p-stops in the p-bulk function more like a wide single piece,

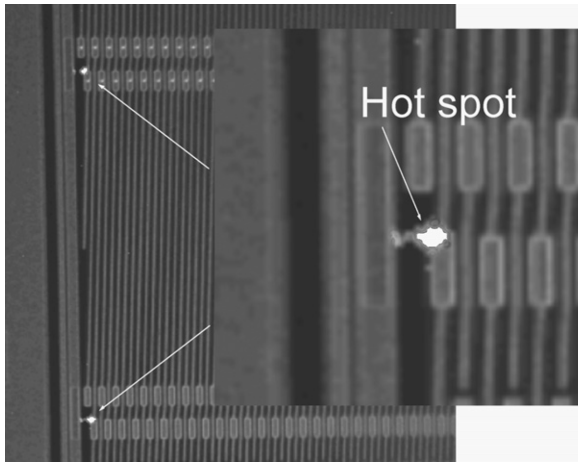

Fig. 7. Hot spots at the end of the stereo strips in the X1R2P8 main sensor observed using the hot-electron equipment.

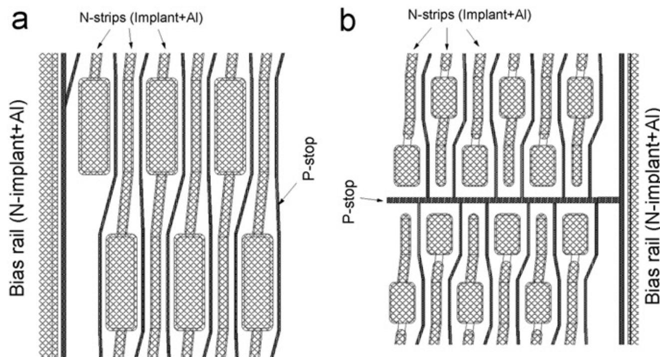

Fig. 8. Mask patterns before modification to eliminate the hot spots in Figs. 6 and 7.

a wider p-stop leads to higher electric field, and a more asymmetric positioning of the p-stop leads to higher electric field.

4.2. Mask modification

In accordance with our understanding of the electric field as per Ref. [14], the PTP structure of X1Z4 was modified to form the structures Z4A–Z4D. For these structures, the n–n distance was increased from 12 to 20 μm. For the Z4A and Z4B structures, the circle of p-top was enlarged towards the p-stops between the n-strips. Thus, the multiple p-stops were placed closer together. For the Z4C structure, the multiple p-stops were compacted into a single continuous p-stop. Finally, for the Z4D structure, the n-island implant was eliminated, making the Z4D structure simple. Although we do not observe a dramatic difference in performance (see Section. 3.3), we investigate further to see if there is a subtle but systematic difference between these structures.

In the main sensor mask, the source of the high electric field is the widely spaced p-stops near the n-strips and the bias rail. This design was only used in the layout of the stereo strips, and we observed no hot spots in the similar corners of the axial strip segments. The mask was modified to eliminate the outermost p-stop near the bias rail and to modify the shape of the bias rail to go along the n-strip edge, so that the distance between the bias rail and the n-strip edge is uniform and the same as in other strips. Drawings of the modified layout for the Fig. 8 (a) and (b) are shown in Fig. 9 (a) and (b), respectively. No n-strip or other p-stop was modified.

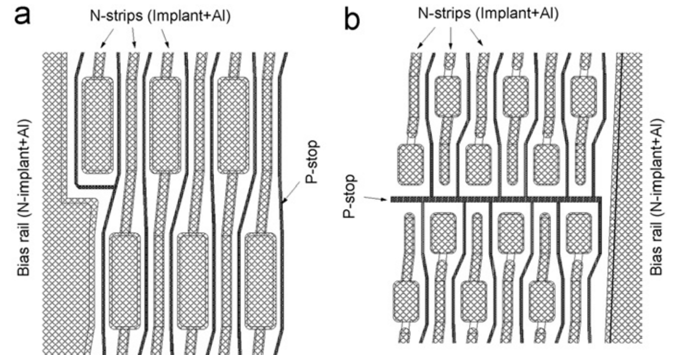

Fig. 9. Mask patterns after modification to eliminate the hot spots in Figs. 6 and 7.

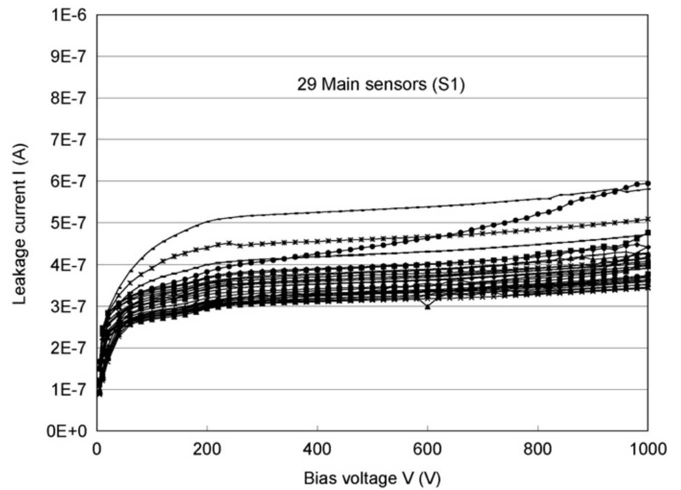

Fig. 10. Leakage currents of the 29 main sensors of the batch S1P4 as a function of bias voltage, measured at room temperature.

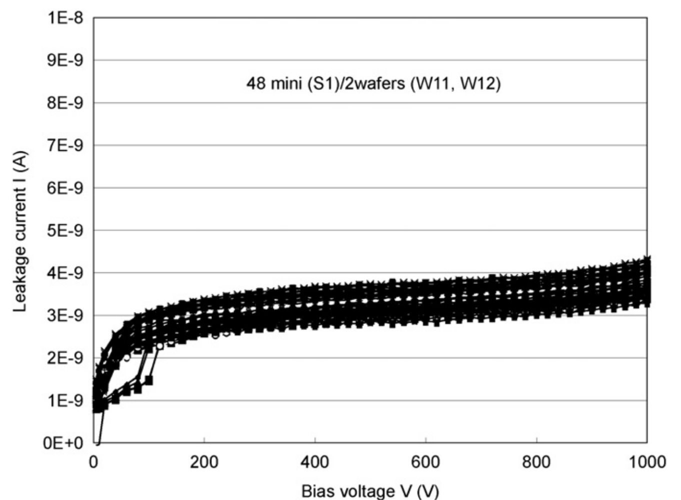

Fig. 11. Leakage currents of 48 miniature sensors from 2 wafers of the batch S1P4 as a function of bias voltage, measured at room temperature. The low current below 100 V in a few samples is an artifact of the measurement device.

4.3. Results after the mask modification

The second batch X2 and later batches were fabricated using the modified mask. We observed good performance and no

microdischarge in the small quantity fabricated, e.g., in batch X3P4 [4]. The *I–V* characteristics of 29 non-irradiated main sensors from the latest batches S1P4 and S1P10, measured at approximately 26 °C, are shown in Fig. 10. Microdischarge is not observed up to the bias voltage of 1000 V. The leakage current is low at less than 0.5 μA or 5 nA/cm^2. The 29 main sensors are equivalent to 2756 miniature sensors of 1 cm × 1 cm in area. The *I–V* characteristics of 48 miniature sensors from the two wafers of S1P4 are shown in Fig. 11. All miniature sensors, including the modified Z4 sensors, exhibit no microdischarge up to 1000 V. Further characterization results of the main sensors are reported in Ref. [7].

5. Summary

We have developed a novel and highly radiation-tolerant n-in-p silicon microstrip sensor for very high radiation environments such as in the SLHC. The sensor is designed for a fluence of 10^{15} neq/cm^2. The goals for this project are also to establish the necessary technological elements to develop a large-area sensor for use in a large-area tracker. We have established a fabrication sequence for fabricating a single 9.75 cm × 9.75 cm large-area sensor with two axial segments and two stereo strip segments and 24 pieces of 1 cm × 1 cm miniature sensors with various n-strip isolation structures. These structures are all laid out on a single p-type, FZ, 6 in. (150 mm) wafer.

We evaluate the sensors both pre- and post-irradiation by protons and neutrons and find that the n-strip isolation depends on the p^+ concentration and that the full depletion voltages evolve to about 800 V. We also report the characterization of the interstrip resistance, interstrip capacitance, the punch-through voltage, etc.

The first fabrication batch allowed us to identify the weak spots in the PTP and in the stereo strip layouts that cause the onset of microdischarge at low bias voltages of 200–400 V. With the help of TCAD simulation, the origin of the weakness was identified and the mask was modified accordingly. The batches after the modification and the latest fabrication of about 30 main sensors with p-stop $\sim 4 \times 10^{12}$ ions/cm^2 and associated miniature sensors have shown good performance, with no microdischarge up to 1000 V.

Acknowledgments

We express our thanks to the team from CYRIC at the Tohoku University and from the TRIGA reactor at the Jozef Stefan Institute for conducting excellent irradiations. The research was partly supported by Ministry of Education, Youth and Sports of the Czech Republic, the German Federal Ministry of Education and Research, the Japan Grant-in-Aid for Scientific Research (A) (Grant no. 20244038), Researh (C) (Grant no. 20540291) and Research on Priority Area (Grant no. 20025007), the Slovenian Research Agency, the Spanish National Program for Particle Physics, the UK Science and Technology Facilities Council (under Grant PP/E006701/1), the US Department of Energy and the US National Science Foundation (under Grant PHY0652607).

References

[1] S. Baranov, et al., Atlas Radiation Background Task Force Summary Document, ATL-GEN-2005-001.
[2] S. Terada, et al., Nucl. Instr. and Meth. A 383 (1996) 159.
[3] G. Casse, et al., Nucl. Instr. and Meth. A 518 (2004) 340.
[4] Y. Unno, Nucl. Instr. Meth. A , doi:10.1016/j.nima.2009.08.008 and references therein.
[5] K. Hara, et al., IEEE Trans. Nucl. Sci. NS-56-2 (2009) 468.
[6] Hamamatsu Photonics K.K., 1126-1 Ichino-cho, Hamamatsu-shi 435-8558, Japan.
[7] J. Bohm, et al., Testing of large area n-in-p silicon sensors intended for a very high radiation environment, Nucl. Instr. and Meth., this issue.
[8] K. Hara, et al., Nucl. Instr. and Meth. A541 (2005) 15.
[9] T. Shinozuka, Y. Unno et al., CYRIC Experiments No. 8512, 8705, 8918, 9136, CYRIC, 6-3 Aramaki-aoba, Aoba-ku, Sendai-shi 980-8578, Japan.
[10] I. Mandic, 〈http://www-f9.ijs.si/~mandic/Reactor.html〉.
[11] K. Hara, et al., Testing of bulk radiation damage of n-in-p silicon sensor for very high radiation environment, Nucl. Instr. and Meth., this issue.
[12] S. Lindgren, et al., Testing of surface properties pre-rad and post-rad of n-in-p silicon sensors for very high radiation environment, Nucl. Instr. and Meth., this issue.
[13] Equipped with a dual-mode cooled CCD camera, Catolog No. C4880-21-26W, Hamamatsu Photonics K.K.
[14] Y. Unno, et al., Optimization of surface structures in n-in-p silicon sensors using TCAD simulation, Nucl. Instr. and Meth., this issue.